Reynolds-Averaged Navier-Stokes Simulation of Absorbency and Tortuosity for Stream through Compressed Absorbent

Dr. R SivaGopal[1], Dr.Y.Madhusudhana Reddy[2]
[1]Assistant Professor, Department of Mathemtics, Sri Venkateswara Institute of Technology, Anantapur. Sivagopal222@gmail.com
[2]Associate Professor, Department of Mathematics, Sri Venkateswara Degree & PG College,Anantapur, Andhra Pradesh, India. ymsmadhu@gmail.com

Abstract
Discrete component technique (DCT) is utilized to deliver thick and fixed permeable media with unbending mono circles. Reynolds Averaged Navier Stokes technique (RANS) is received to recreate the liquid stream in timespan circles. To reenacting a similar actual issue, the porousness is gotten with various grid numbers. We confirm that the porousness is immaterial to the body power and the media length along stream bearing. The connections between penetrability, convolution and porosity, and circle span are explored, and the outcomes are contrasted and those detailed by different creators. The acquired outcomes demonstrate that RANS is fit to liquid stream reproduction of permeable media because of its innate hypothetical benefits. The sweep of circle ought to have ten cross sections in any event and the media length along stream course ought to be in excess of twenty radii. The power has no impact on the coefficient of penetrability with the limit of moderate liquid stream. For mono circles permeable media test, the relationship of penetrability and porosity concurs well with the K-C condition, and the convolution diminishes straightly with expanding porosity.
Keywords: Reynolds Averaged Navier Stokes Techniques– Tortuosity

Introduction

As of late, the size and stature of regular level breeze turbines have not stopped to increment considering saddling ever bigger amounts of wind energy. This expansion anyway carries primary difficulties to the plan of future breeze turbines. One of the promising choices to outfit wind energy at expanding heights is to utilize a flying gadget that is fastened to the ground. There are various ideas and methods of activity of such airborne breeze energy (AWE) gadgets [1]. A conspicuous model is to fly a wing crosswind and tie it to a generator on the ground. The streamlined power on the wing reels out the tie and turns a drum, henceforth creating mechanical force that can be changed over to electrical force. Albeit these AWE gadgets present a few benefits contrasted with regular breeze turbines, they face likewise numerous difficulties for enormous scope business arrangement. One of them is identified with the absence of information and reference information concerning the streamlined features of such wings. The comprehension of the stream elements past the wing is anyway critical to further develop the framework plan and, partly, identify with the primary distortions saw during airlift.

$$k_{ij} = -\frac{\gamma^{\mu}}{p_{,i}}\langle v_j \rangle \qquad (1.1)$$

Where v_j surge speed toward the path j, $\langle\rangle$ is addresses volume normal, γ^{μ} is the thickness coefficient of the liquid, $p_{,i}$ is the pressing factor slope in heading i, and k_{ij} is the penetrability network. Penetrability lattice is thought to be inclining and positive distinct. The components of penetrability lattice can be estimated by trial techniques or assessed by computational strategies. When $\mu = 0$, yeilds the result obtained by Ping wang that is the lattice Boltzmann simulation pf permeability and tortuosity for flow through dense porous media.
Numerous elements influence porousness, for example, permeable media structure, liquid actual properties, and level of liquid immersion. This paper examines the effect of permeable media structure as it were. The customary prescient exploration is generally worried about the connection among porousness and porosity. Moreover, explicit surface of the molecule, state of the molecule, and convolution additionally have a critical sway on penetrability. In any case, impacts of these elements are hard or even difficult to quantify precisely; these issues need pore-scale reenactment of liquid stream in permeable media. On account of the intricacy of liquid stream in permeable media, aside from some extremely basic inquiry, it is hard to get the scientific arrangement. With the advancement of the permeable media math representation, registering power, and computational techniques, it is feasible to mimic straightforwardly liquid stream in pore-scale permeable media.

The RANS technique has been applied to this field since it was presented before LBM. Ghassemi and Pak [2] examined the impacts of penetrability and convolution on move through particulate media by RANS and DCT; the connections between porousness furthermore, convolution with different boundaries like particles distances across, grain explicit surface, and porosity were distinguished. The outcomes show that the connection among penetrability and porosity of the permeable media concurred the K-C recipe well, yet there is a piece deviation in the high porosityconvolution straightly diminishes with the porosity and the molecule measurement doesn't influence convolution any more after it turns out to be sufficiently enormous.

Sun et al. [3] presented a multiscale strategy, Microstructural credits, for example, blocked/associated porosity and mathematical convolution are separated utilizing new computational procedures to frame computerized pictures of permeable media, and a RANS conspire is utilized to get homogenized successful porousness at example scale.
The outcomes show that the penetrability depends not just on the porosity, yet additionally on the availability and the convolution. Trial estimations and RANS reenactment on tests of stuffed molecule beds were investigated by Videla et al. [4]. Because of as far as possible, when the molecule distance across is more prominent than 500 microns, the trial results perhaps mathematical outcomes are steady. The effect of the unwinding time on penetrability was likewise examined. Vidal et al. [5] confirmed that the LBM mathematical porousness of the permeable media of round particles concurs with trial information quite well. At the point when the size conveyance of circular particles scatters partially, the outcomes start to veer off fromK-C recipe, and an altered equation was given as per the outcomes. Jeong [6] contemplated the miniature streams through granular porousmedia at different Knudsen numbers, the connection between's the porousness, the porosity, and

the Knudsen number is inferred, another fitting equation is given, and the impact of rarefaction on the penetrability is moreover talked about. Van der Hoef et al. [7] recreated liquid stream past mono-and bidisperse arbitrary varieties of circles with RANS, the determined penetrability is steady with test results, and another drag power recipe is given. The impact of the plan of the particles and molecule shape on penetrability anisotropy was investigated by Stewart et al. [8].

2 Methodology

2.1 Discrete component technique

Discrete component technique (DCT) is an unequivocal mathematical technique for displaying movement of unmistakable particles. Since this technique was presented by Cundall and Strack [9], it has become an integral asset and has been utilized to investigate a wide scope of issues in science and designing. In DCT, the granular permeable media are viewed as an get together of unmistakable inflexible particles. At the point when cross-over happens between particles (or molecule and divider), the contact power isolates them from one another. Utilizing the power removal law, the power arrangement of every molecule can be added. The removal and speed of every molecule can be determined by Newton's second law of movement. The power relocation law gives the relationship between the contact power and the cross-over between particles
(or on the other hand molecule and divider) by the accompanying conditions:

$$\frac{\partial \gamma}{\partial t}+\frac{\partial \gamma u_j}{\partial x_j}=P_\gamma-D_\gamma+\frac{\partial}{\partial x_j}\left[\left(\nu+\frac{\nu_t}{\sigma_f}\right)\frac{\partial \gamma}{\partial x_j}\right] (2)$$

$$P_\gamma = F_{\text{length}}\, c_{a1}\left|\frac{\partial u}{\partial u}\right| (\gamma F_{\text{onset}})^{\frac{1}{2}}(1-c_{e1}\gamma) \quad (3)$$

Newton's second law ofmotion portrays the relationship between the acting powers and development of molecule. For circle p, the law peruses

$$m_p \ddot{x}_{p,i}=\sum\left(F^{\tau}_{p,i}+F^{n}_{p,i}\right)-F^{d}_{p,i}$$
$$I_p \ddot{\theta}_{p,i}=\sum\left[\left(\mathbf{F}^{\tau}_{p}\times\mathbf{R}_p\right)_i\right]-M^{d}_{p,i} \quad (4)$$

where the function F_{length} controls the transition length and its correlation is given in [15], and y is the distance from the nearest wall. Furthermore, γF_{onset} t controls the transition onset and quickly grows from 0 to 1 when the boundary layer becomes turbulent, based on the ratio between the vorticity Reynolds number and the critical momentum thickness Reynoldsnumber Re_c. The expression for the latter is also given by a correlation, as detailed in [15].

Both correlations for $R_{e\theta_c}$ and F_{length} are a function of the local transition onset momentumthickness Reynolds number $R_{e\theta_t}$.The function γF_{onset} activates an intermittency source term and leads to turbulence production. The destruction term, or relaminarisation source, is defined as

$$D_\gamma = c_{a2}\Omega\gamma F_{\text{turb}}\,(c_{e2}\gamma-1) \quad (5)$$

where Ω represents the vorticity greatness. The capacity F_{turb} is intended to cripple irregularity obliteration outside of the laminar limit layer or in the thick sublayer and is given by

$$F_{\text{turb}} = e^{\left(-\frac{R_T}{4}\right)^4} \quad (6)$$

Finally, the intermittency is modified to be able to exceed $\gamma = 1$ during the laminar boundary layer separation, in order to improve the prediction of separation-induced transition. Thus, we have

$$\gamma_{\text{sep}} = min\left(s_1 max\left[0, \left(\frac{\text{Re}_v}{3.235\, Re_{Ac}}\right) - 1\right] F_{\text{reattach}}, 2\right) F_{\theta t} \quad (7)$$

A second vehicle condition is planned for the neighbourhood change beginning energy thickness Reynolds number $\widetilde{\text{Re}}_{\theta t}$ and is communicated as

$$\frac{\partial \widetilde{\text{Re}}_{\theta t}}{\partial t} + \frac{\partial \tilde{\text{R}}e_{\theta t} u_j}{\partial x_j} = P_{\theta \text{t}} + \frac{\partial}{\partial x_j}\left[\sigma_{\theta t}(\nu + \nu_t)\frac{\partial \widetilde{\text{Re}}_{\theta t}}{\partial x_j}\right] \quad (8)$$

2.2. Permeable Media Generation Using DEM.

The initial step of displaying is creating thick with mesh get together of granular particles.. The subtleties are displayed in Figures 1 and 2. An area whose size is 100 × 100 × 1000 by cross section unit is made first. Occasional limit condition is utilized in the two even ways. In vertical heading, unbending and blocked planes are set at the top and base limits. The inflexible particles are made in a little area close the top limit first, to diminish the likelihood of cross-over; the proportion of particles volume to space is set to ten percent.The position of every molecule will be resolved at the point when it doesn't cover with some other particles. Since the level of particles is low, this interaction is not difficult to execute.

After the free get together is made in the particular locale, it simulates the flow of leading edge inflatable wing for air bond wing (Figure 1). When the particles leave the underlying locale absolutely, new particles will be made. This interaction is rehashed until enough particles show up in computational area. The particles cooperate with other particles and the thick get together of particles frames under gravity finally. To get free permeable media with an ideal porosity, the radii of particles are abbreviated with same scale, however the sum and places of particles are unaltered.

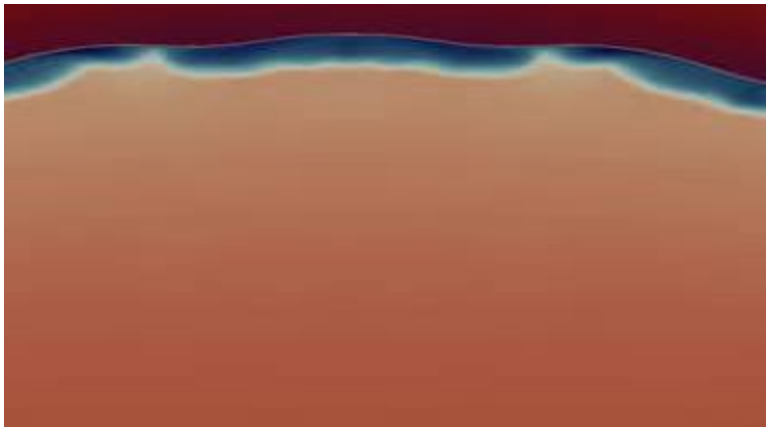

Figure 1: simulates the flow of leading edge inflatable wing for air bond wing

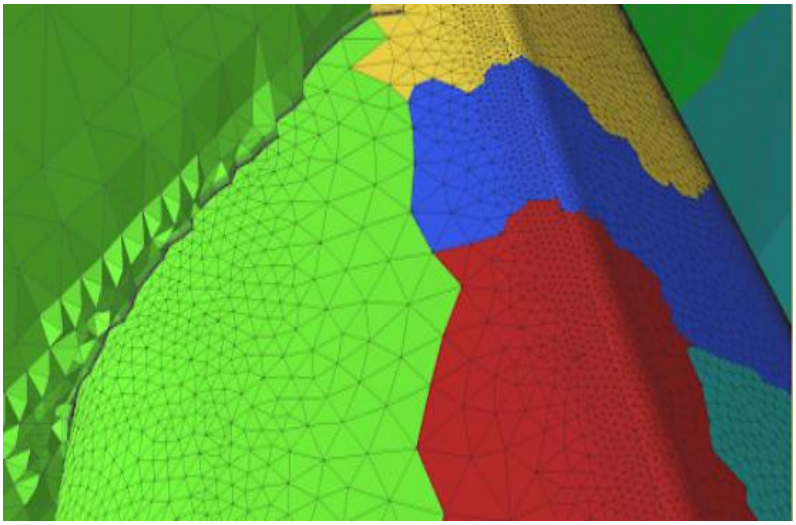

Figure 2: Surface Parallel Mesh

A half and half organized and unstructured lattice was created utilizing the T-Rex calculation of lattice age programming Pointwise R . This uses a organized cross section in the limit layer and close divider area, and an unstructured lattice. The itemized fitting method is depicted in [8]. The surface cross section of the wing and the volume cross section of the computational area are displayed by several authors, individually. A cross section intermingling study was performed with six different networks yet keeping the tallness of the littlest cell near the wing limit to such an extent that $y+ < 1$. It was discovered that a lattice with 330 focuses along the main edge in the spanwise heading, 120 focuses along the airfoil prole, and a cell development proportion of 1:15 in the limit layer, prompts saintly precise what's more, met results. Generally, this gives a cross section containing roughly 6 million cells and this was utilized for every one of the outcomes introduced in this paper. At the bay, the size of the speed weld is set to solidarity and its bearing shifts relying upon the ideal approach.

The pressing factor angle is set to nothing. The disturbance power is set to 0:02 and the proportion of swirl consistency to actual thickness approaches ten. At long last γ= 1 and $R_{e\theta t}$ is determined utilizing the exact relationships. At the power source, the pressing factor is set to nothing and a zero angle is recommended for the speed empirical calculations and the disturbance amounts. A no-slip limit condition is applied at the wing surface. At the dividers, both γ and also$\check{R}_{e\theta t}$, experience a zero typical flux. The model requires that thirst cell close to the divider satisfies positive y approximately equal to one, to catch the temporary limit layer enough. At long last, a balance limit condition is forced at the plane of balance, so that lone portion of the wing is demonstrated.

3. Results

Figure 3 shows the lift and drag polars of the three-dimensional wing for a scope of Reynolds numbers $11^5 \leq R \leq 16 * 11^6$ and approaches shifting somewhere in the range of $-7°$ and $23°$It is significant that, because of the decision of solver that is consistent express, the outcomes for approaches before slow down are considered generally dependable. The outcomes at slow down and post-slow down are for the most part characteristic, realizing that a similar model gave precise outcomes in these conditions for the two-dimensional flow past a sailwing [10]. In Fig. 3, it is evident that the most reduced considered Reynolds number of $Re = 11^5$gives significantlydifferent results than the others, as ow partition happens

straightforwardly from a laminar limit layer. The approach at which slow down happens increments with *Re*, until$Re = 11^7$, so, all in all it diminishes until Re = 107. For Re > 107, the slow down point and greatest lift coecient increment once more. Curiously, this conduct was at that point saw in the two-dimensional reproductions of [10]. This conduct can be clarified by the system of ow progress and can accordingly possibly be caught when a change model is utilized. Previously giving more knowledge into the instrument of ow change, reproduction results with and without progress models are analyzed. Figure 4 shows the lift (left) and drag (right) coefficients at three Reynolds numbers with (strong line) and without (ran line) progress model. It is shown that the lift and drag coefficients with and without progress model concur well for points of assault before slow down for all the Reynolds numbers considered. At slow down, be that as it may, inconsistencies are gotten for both the lift and drag coefficient for $Re = 5 * 11^5$and$Re = 3 * 11^6$. True to form, the requirement for a change model reductions at higher Reynolds numbers. Comparable perceptions are made while breaking down the skin grating coecient at the outside of the wing.

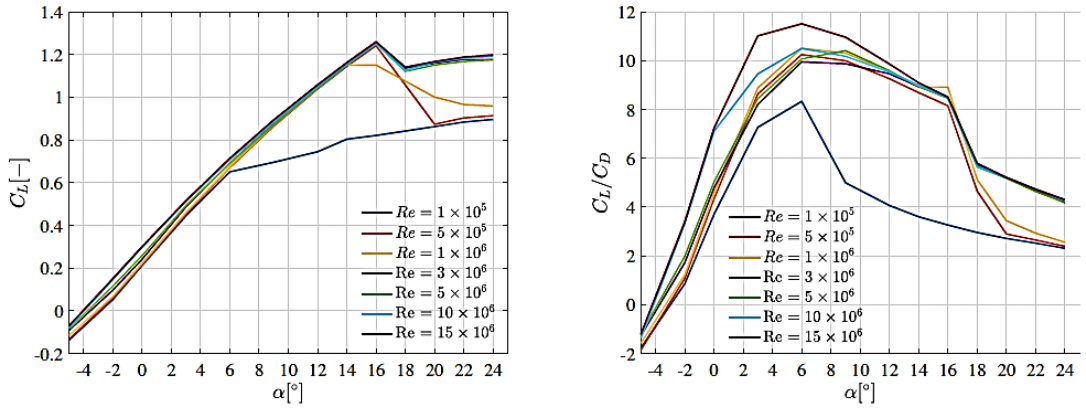

Figure 3: High coefficient (left) and ratio of High-to-low coefficients (right) for the LEI wing calculated at numerous Reynolds numbers.

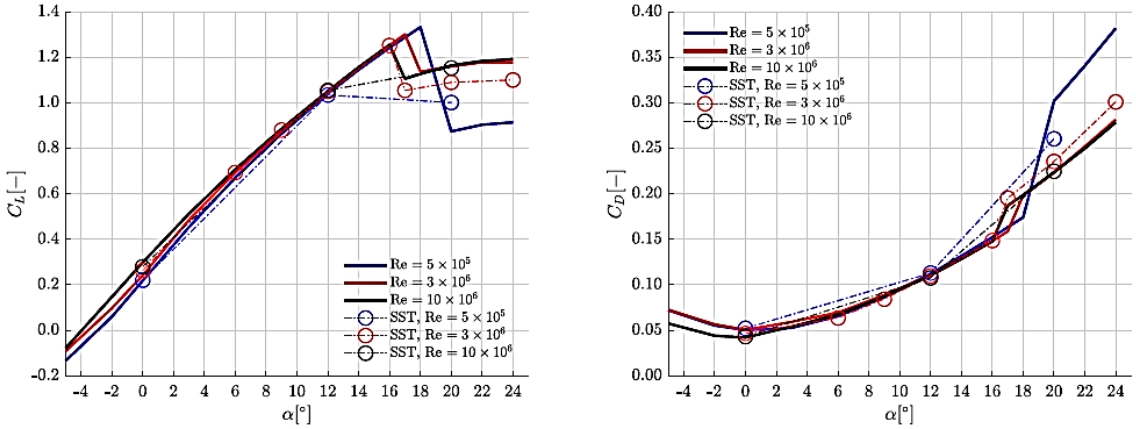

Figure 4: High (left) and slog (right) polars for the LEI wing computed at several Reynolds numbers, with (solid line) and without (dashed line) conversionclassic[8].

4. Conclusion

This work gives mathematical information to the streamlined exhibition of a main edge in atable wing under a scope of flow conditions that are delegate for the activity of airborne breeze energy frameworks. The re-enactments were performed utilizing a consistent state RANS solver with a $k-\omega$SST disturbance model and a low progress model. It is shown that the progress model was needed to precisely foresee the event of slow down up to basically$Re = 3 * 11^6$. It is significant to note, notwithstanding, that the current outcomes at slow down and post-slow down conditions ought to be thought of with care because of the utilization of a consistent state solver. Further work is required at these conditions utilizing temperamental and higher models to confirm the current outcomes. In spite of the limits of the solver, the polars show comparative patterns to the consequences of a two-dimensional flow past a LEI airfoil. The outcomes likewise feature a lot of cross flow along the range of the wing. At long last, extra bits of knowledge are furnished dependent on an examination with in light estimations. In future work, the influence of the presence of swaggers on the wing will likewise require to be additionally researched.

References :

[1] H. Darcy, Determination des Lois d' Ecoulement de l'eau a Travers le Sable,, Les Fontaines Publiques de la Ville de Dijon, Victor Dalmont, Paris, France, 1856.

[2] A. Ghassemi and A. Pak, "Pore scale study of permeability and tortuosity for flow through particulate media using Lattice Boltzmann method," International Journal for Numerical and Analytical Methods in Geomechanics, vol. 35, no. 8, pp. 886–901, 2011.

[3] W. C. Sun, J. E. Andrade, and J. W. Rudnicki, "Multiscale method for characterization of porous microstructures and their impact on macroscopic effective permeability," International Journal for Numerical Methods in Engineering, vol. 88, no. 12, pp. 1260–1279,2011.

[4] A. R. Videla, C. L. Lin, and J. D. Miller, "Simulation of satu- rated fluid flow in packed particle beds—the lattice-Boltzmaan method for the calculation of permeability from XMT images," Journal of the Chinese Institute of Chemical Engineers, vol. 39, no. 2, pp. 117–128,2008.

[5] D. Vidal, C. Ridgway, G. Pianet, J. Schoelkopf, R. Roy, and F. Bertrand, "Effect of particle size distribution and packing compression on fluid permeability as predicted by lattice- Boltzmann simulations," Computers and Chemical Engineering, vol. 33, no. 1, pp. 256–266, 2009.

[6] N. Jeong, "Advanced study about the permeability for micro- porous structures using the lattice Boltzmann method," Trans- port in Porous Media, vol. 83, no. 2, pp. 271–288, 2010.

[7] M. A. van der Hoef, R. Beetstra, and J. A. M. Kuipers, "Lattice-Boltzmann simulations of low-Reynolds-number flow past mono- and bi-disperse arrays of spheres: results for the permeability and drag force," Journal of Fluid Mechanics, vol. 528, pp. 233–254,2005.

[8] M. L. Stewart, A. L. Ward, and D. R. Rector, "A study of pore geometry effects on anisotropy in hydraulic permeability using the lattice-Boltzmann method," Advances in Water Resources, vol. 29, no. 9, pp. 1328–1340, 2006.

[9] P. A. Cundall and O. D. L. Strack, "The distinct numerical model for granular assemblies," Geotechnique, vol. 29, no. 1, pp. 47–65, 1979.

[10] P. L. Bhatnagar, E. P. Gross, and M. Krook, "A model for collision processes in gases. I. Small amplitude processes in charged and neutral one-component systems," Physical Review, vol. 94, no.3, pp. 511–525, 1954.

[11]R.C. Leuthold. Multiple-wake vortex lattice method for membrane wing kites. Master's thesis, Delft University of Technology, 2015.

[12]O. Lorillu, R. Weber, and J. Hureau. Numerical and experimental analysis of two-dimensional separated flows over a flexible sail. J. Fluid Mech.,466(1):319–341, 2002.

[13]F. Menter and T. Esch. Elements of industrial heat transfer prediction. Proceedings of the 16th Brazilian Congress of Mechanical Engineering (COBEM), 2001.

[14]F.R. Menter. Two-equation eddy-viscosity turbulence models for engineering applications. AIAA J., 32(8):1598–1605, 1994.

[15]J. Oehler and R. Schmehl. Aerodynamic characterization of a soft kite by in situ flow measurement. Wind Energy Science, 4(1):1–21, 2019.

[16]J. Oehler, M. van Reijen, and R. Schmehl. Experimental investigation of soft kite performance during turning maneuvers. Journal of Physics: Conference Series, 1037(052004), 2018.

[17]B. Python. Methodology improvement for performance assessment of pumping kite power wing. Master's thesis, Delft University of Technology and Ecole Polytechnique F´ed´erale de Lausanne, 2017.

[18]Mostafa A. Rushdi, Ahmad A. Rushdi, Tarek N. Dief, Amr M. Halawa, Shigeo Yoshida, and Roland Schmehl. Power prediction of airborne wind energy systems using multivariate machine learning. Energies, 13(9), 2020.

[19]S. Sachdeva. Impact of turning-induced shape deformations on aerodynamic performance of leading edge inflatable kites. Master's thesis, Delft University of Technology, 2017.